Intermediate-band solar cells: Influence of band formation on dynamical processes in InAs/GaAs quantum dot arrays

Stanko Tomić*
Computational Science and Engineering Department, STFC Daresbury Laboratory, Cheshire WA4 4AD, United Kingdom
(Received 12 July 2010; revised manuscript received 6 October 2010; published 19 November 2010)

We present a theoretical model for design and analysis of semiconductor quantum dot (QD) array-based intermediate-band solar cell (IBSC). The plane-wave method with periodic boundary conditions is used in expansion of the $\mathbf{k}\cdot\mathbf{p}$ Hamiltonian for calculation of the electronic and optical structures of InAs/GaAs QD array. Taking into account realistic QD shape, QD periodicity in the array, as well as effects such as band mixing between states in the conduction and valence band, strain and piezoelectric field, the model reveals the origin of the intermediate-band formation inside forbidden energy gap of the barrier material. Having established the interrelation between QD periodicity and the electronic structure across the QD array Brillouin zone, conditions are identified for the appearance of pure zero density-of-states regions, that separate intermediate band from the rest of the conduction band. For one realistic QD array we have estimated all important absorption coefficients in IBSC, and most important, radiative and nonradiative scattering times. Under radiative-limit approximation we have estimated efficiency of such IBSC to be 39%.

DOI: 10.1103/PhysRevB.82.195321 PACS number(s): 73.21.La, 78.66.Fd, 84.60.Jt

I. INTRODUCTION

Conventional single-energy-gap solar cells (SCs) have an ultimate efficiency limit that was established by Shockley and Queisser (SQ)[1] on the basis of detailed balance arguments. The "balance" in the model comes from the fact that it quantitatively accounts for two opposing fundamental processes that occur in any SC: absorption and emission. For SC at room temperature the maximum efficiency is further reduced to 40.7% with $E_g=1.1$ eV under maximum concentration condition and to 31% with a $E_g=1.3$ eV, at one sun (i.e., when the solid angle subtended by the sun shining on a cell at normal incidence is taken into account). The main reason underlying those values is that only photons with an energy close to that of the semiconductor E_g are effectively converted. Photons with lower energy then E_g are simply lost (the semiconductor is transparent to them); and out of the photons with higher energy ($>E_g$), only a part of their energy, i.e., that equals the E_g energy is at best converted. The majority of high-energy electrons generated by photons with $>E_g$, (hot carriers) decay thermally to the Fermi level of the conduction band before they can contribute to the current.

The principal aim, to increasing efficiency of SC, must be to make better use of the solar spectrum.[2–4] One such improvement is to take advantage of the incident photons with subband gap energy to be absorbed and contribute to increase photocurrent while in the same time the output voltage of device would ideally be preserved at its maximal value that is determined by the largest E_g that exists in the system (i.e., host material energy gap). A possible solution to that problem emerged in the form of *intermediate-band solar cell* (IBSC) scheme.[5–7] The limiting efficiency of the IBSC concept for full concentration and at room temperature is 63.2% with optimized absorption energies at ~1.2, ~0.7, and ~1.9 eV,[5] significantly overcoming the SQ limit of 40.7% for a conventional single-gap SC under the same operating conditions.

Conceptually, an IBSC is manufactured by sandwiching an intermediate-band (IB) material between two selective contacts, of p and n types (Fig. 1). The IB material is characterized by the existence of an electronic energy band of allowed states within the conventional-energy band gap E_g of the host material, splitting it into two subgaps, E_{gL} and E_{gH}. This band allows the creation of additional electron-hole pairs from the absorption of two subband gap energy photons. Under this assumption, first photon (1) pumps an electron from the valence band (VB) to the IB, and a second photon (2) pumps an electron from the IB to the conduction band (CB). To this end, it is necessary that the IB is half filled with electrons so that it can supply electrons to the CB as well as receive them from the VB. This two-photon absorption process is also illustrated in Fig. 1 and has been experimentally detected in IBSCs based on quantum dots.[8] The electron-hole pairs generated in this way add up to the conventionally generated ones by the absorption of a single photon (3), the third one, pumping an electron from the VB to the CB. Therefore, the photocurrent of the solar cell and ultimately its efficiency are enhanced since this increment in photocurrent occurs without degradation of the output voltage of the cell. The output voltage is given by the split between electron and hole quasi-Fermi levels, E_{F_C} and E_{F_V}, that is still limited by the total band gap E_g.[9–12] The robustness of

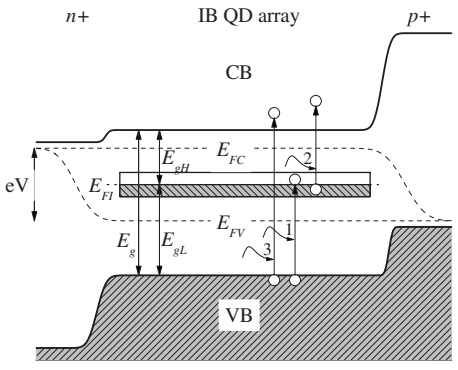

FIG. 1. Schematic view of the IBSC band diagram.

the IBSC concept allows for various energy-gap combinations to be found that provides for very similar efficiency. This is of particular importance for QD-based designs as it opens up a much larger design space for IB solar cells.[13]

So far the maximum conversion efficiency of the IBSC experimentally measured was 18.3% reported by Blokhin *et al.*[14] Their device was based on AlGaAs/GaAs single-junction photovoltaic cells with an array of vertically coupled InGaAs QDs. Even more fascinating, this results was for the unconcentrated ground-level solar spectrum.

In this paper we describe theoretical methods for design, and discuss possibility of using, semiconductor QD as an absorbing medium in IBSCs. In the QD implementation of IBSCs the intermediate band is created inside host semiconductor (barrier) material by three-dimensional periodic array of QDs. In reality, it is rather a one-dimensional array of vertically aligned QDs.[14–24] For each electron-bound energy level available inside a single QD, a periodic array of such QDs will produce a miniband. Those minibands will lie inside the forbidden energy gap of the barrier material. If there is only one bound energy level in the CB of QD, this may become the IB. With proper *prefilling* or *photofilling*, the quasi-Fermi level can be positioned within the IB.[25] In this way, the IB can be half full, providing coexistence of filled and empty states in the IB, and enhancing the probability of creating photogenerated carriers.

In the IBSC design based on QD structures the requirement for band formation can be relaxed as a single QD level can be equally as good if the Fermi level is on (or near) it. Indeed if the IB is enough wide (very close QD packing) there may be transport along the stacks of QDs. The most of the desirable transport in the QD-IBSC takes place within the CB and VB while the IB transport is not as important.[26] Throughout this paper all relevant physical properties of the IBSC were reported for single QD in the isolation (that are technologically more feasible) and for the QD array made of the same size QDs.

The paper is organized as follows: after introduction, Sec. I, in the second part, Sec. II, we review theoretical methods for the calculation of electronic and optical properties of the QD array used for IBSCs. In Sec. II A we briefly outline the $\mathbf{k}\cdot\mathbf{p}$ theory and its eight-band implementation, as a method used for quantum-mechanical treatment of electronic structure of strained semiconductor QD arrays. In Sec. II B we discuss advantages of the plane-waves expansion method combined with periodic boundary conditions for the calculation of the electronic structure of QD arrays. In Sec. III A, we introduce the model QD array used throughout this work. In Sec. III B we discuss the origin of intermediate-band formation in QD arrays which is followed by the analysis of the electronic structure of QD arrays in Sec. III C. Results presented in Secs. III B and III C are used then to examine the absorption characteristics of QD arrays. In Sec. IV, we discuss dominant radiative and nonradiative processes that might influence successful operation of QD array-based IBSC. It includes theory of radiative processes in Sec. IV A, theory of electron-phonon scattering processes in Sec. IV C, and theory of the two most important nonradiative Auger processes: electron cooling and biexitonic recombination discussed in Sec. IV B. In Sec. V we give concluding remarks.

II. THEORY OF QD ARRAY ELECTRONIC STRUCTURE

A. $\mathbf{k}\cdot\mathbf{p}$ theory

The quantum-mechanical description of electrons in IBSC requires detailed knowledge of their wave functions, $\psi_{n,\mathbf{k}}(\mathbf{r})$, which are found by solving the Schrödinger equation (in the single-electron approximation)

$$H_0\psi_{n,\mathbf{k}}(\mathbf{r}) = E_{n,\mathbf{k}}\psi_{n,\mathbf{k}}(\mathbf{r}). \tag{1}$$

The Hamiltonian in Eq. (1), $H_0 = p^2/2m_0 + V(\mathbf{r})$, is the function of the quantum-mechanical momentum operator, $\mathbf{p} = -i\hbar\nabla$, and the crystal potential experienced by electrons, $V(\mathbf{r}) = V(\mathbf{r}+\mathbf{R})$, which is a periodic function, with the periodicity of the crystal lattice, $\mathbf{R}$. According to Bloch's theorem, the solutions to this Schrödinger equation can be written as: $\psi_{n,\mathbf{k}}(\mathbf{r}) = e^{i\mathbf{k}\cdot\mathbf{r}}u_{n,\mathbf{k}}(\mathbf{r})$, where $\mathbf{k}$ is electron wave vector, n is the band index, and $u_{n,\mathbf{k}}$ is the *cell-periodic* function with the same periodicity as the crystal lattice. The cell-periodic function, $u_{n,\mathbf{k}}$, satisfies equation

$$H_{\mathbf{k}}u_{n,\mathbf{k}} = E_{n,\mathbf{k}}u_{n,\mathbf{k}}, \tag{2}$$

where the Hamiltonian

$$H_{\mathbf{k}} = H_0 + H'_{\mathbf{k}} = \frac{p^2}{2m_0} + V + \frac{\hbar^2k^2}{2m_0} + \frac{\hbar\mathbf{k}\cdot\mathbf{p}}{m_0} \tag{3}$$

is given as a sum of two terms: the unperturbed, H_0, which, in fact, equals the exact Hamiltonian at $\mathbf{k}=0$ (i.e., at the Γ point in the Brillouin zone) and the "perturbation," $H'_{\mathbf{k}}$. Equation (3) is called the $\mathbf{k}\cdot\mathbf{p}$ Hamiltonian.[27–29] The perturbation term $H'_{\mathbf{k}}$ gets progressively smaller as $\mathbf{k}$ approaches zero. Therefore, the $\mathbf{k}\cdot\mathbf{p}$ perturbation theory is most accurate for small values of $\mathbf{k}$. However, if enough terms are included in the perturbative expansion, then the theory can, in fact, be reasonably accurate for any value of $\mathbf{k}$ in the entire Brillouin zone.[30–34] The parameters required to do these calculations, are the band edge energies, $E_{n,0}$, and the optical matrix elements, $\langle u_{n,0}|\mathbf{p}|u_{n',0}\rangle$, are typically inferred from experimental data and detailed atomistic-based theories.[35]

A particular strength of the $\mathbf{k}\cdot\mathbf{p}$ theory is straightforward inclusion of the spin-orbit (SO) interaction and of strain effects on the band structure via deformation potential theory.[36] Relativistic effects in the $\mathbf{k}\cdot\mathbf{p}$ method are included perturbatively via the SO interaction Hamiltonian, $H_{\mathrm{SO}} = (2\Delta/3\hbar^2)\mathbf{L}\cdot\mathbf{S}$, where $\mathbf{L}$ is the orbital angular momentum operator and $\mathbf{S}$ is the spin operator, and Δ is the spin-orbit split energy. In a strained system the coordinate axes are stretched or compressed.[36] Therefore, the coordinates are transformed as: $\mathbf{r}' = (1+\epsilon)^{-1}\cdot\mathbf{r}$, where $\mathbf{r}$ is the unstrained coordinate, assuming only effects up to the first order in strain tensor ϵ. Consequently the translational symmetry of the new, *strained cell-periodic functions*, $\tilde{u}_{n,\mathbf{k}'}(\mathbf{r}') = u_{n,\mathbf{k}}([1+\epsilon]^{-1}\cdot\mathbf{r})$, is associated with the wave vector, $\mathbf{k}' = (1+\epsilon)\cdot\mathbf{k}$. By solving the $\mathbf{k}\cdot\mathbf{p}$ equation in the new coordinate system defined by $(\mathbf{k}',\mathbf{r}')$, and using modified Bloch $\tilde{\psi}_{n,\mathbf{k}'}(\mathbf{r}')$, and cell-periodic $\tilde{u}_{n,\mathbf{k}'}(\mathbf{r}')$, functions, and neglecting all second-order effects due to strain tensor, ϵ, the strained $\mathbf{k}\cdot\mathbf{p}$ Hamiltonian becomes

$$H_{\mathbf{k}} = \frac{p^2}{2m_0} + V + \frac{\hbar^2 k^2}{2m_0} + \frac{\hbar \mathbf{k}\cdot\mathbf{p}}{m_0} + \frac{1}{4m_0^2 c^2}(\vec{\sigma}\times\nabla V)\cdot(\mathbf{k}+\mathbf{p}) + \mathbf{D}^{\epsilon}\cdot\epsilon, \quad (4)$$

where the $\mathbf{D}^{\epsilon}$ is the deformation potential operator and $\vec{\sigma} = (\sigma_x, \sigma_y, \sigma_z)$ is a vector consisting of the three Pauli spin matrices.[37]

The theoretical model of the QD array electronic structure, used in this paper, is based on the eight-band $\mathbf{k}\cdot\mathbf{p}$ implementation[38] of Hamiltonian (4) adapted for QD nanostructures.[39,40] This Hamiltonian takes into account band mixing between the lower conduction band *s*-antibonding and top three valence-band *p*-bonding states, all spin degenerate, in the underlying QD and barrier materials, and includes the strain and piezoelectric field. It is established that such Hamiltonian once implemented for periodic structures (see Sec. II B) gives excellent agreement with the experimental results on the confined energies in the InAs/GaAs QD array system obtained by photoreflectance and electroluminescence measurements.[7,41–43]

B. Plane-waves implementation of QD array electronic structure solver

The QD as a three-dimensional (3D) object breaks the translational symmetry of the bulk material along all three Cartesian directions implying operator replacement $k_\nu \rightarrow -i\partial/\partial\nu$ in Eq. (4), where $\nu=(x,y,z)$. To solve the multiband system of Schrödinger equations, Eq. (4), the plane-wave (PW) methodology is employed as an expansion method.[44–47] In the PW representation the eigenvalues (E_n) and coefficients ($A_{n,\mathbf{k}}$) of the nth eigenvector, $[\psi_n(\mathbf{r}) = \Sigma_{\mathbf{k}} A_{n,\mathbf{k}} e^{i\mathbf{kr}}]$, are linked by the relation

$$\sum_{m,\mathbf{k}'} h_{m,n}(\mathbf{k}',\mathbf{k}) A_{n,\mathbf{k}} = E_n \sum_{\mathbf{k}} A_{n,\mathbf{k}}, \quad (5)$$

where $h_{m,n}(\mathbf{k}',\mathbf{k})$ are the Fourier transform of the Hamiltonian matrix elements, and $m,n \in \{1,\ldots,8\}$ are the band indexes of the eight-band $\mathbf{k}\cdot\mathbf{p}$ Hamiltonian. All the elements in the Hamiltonian matrix, Eq. (5), can be expressed as a linear combination of different kinetic and strain-related terms and its convolution with the characteristic function of the actual QD shape, $\chi_{\mathrm{qd}}(\mathbf{k})$.[47,48] The whole $\mathbf{k}$ space is discretized by embedding the QD in a rectangular box of dimensions L_x, L_y, and L_z and volume $\Omega = L_x \times L_y \times L_z$ and choosing the $\mathbf{k}$ vectors in the form of $\mathbf{k} = 2\pi(n_x/L_x, n_y/L_y, n_z/L_z)$, where n_x, n_y, and n_z are integers whose change controls the convergence of the method.

The PW-based $\mathbf{k}\cdot\mathbf{p}$ method inherently assumes *periodic Born-von Karman boundary conditions* and is particularly suited for analysis of the QD array structures. The electronic structure of such an array is characterized by a Brillouin zone (BZ) determined by the QD array dimensions.[41,49–52] To calculate the electronic structure the only modification to the basis set is to replace the reciprocal lattice vectors in the PW expansion with those shifted due to the QD-superlattice (QD-SL)

$$k_\nu \rightarrow k_\nu + K_\nu, \quad (6)$$

where $0 \le K_\nu \le \pi/L_\nu$ and the L_ν are the superlattice vectors in the $\nu=(x,y,z)$ directions and corresponds to those forming the volume Ω. This allows sampling along the $\mathbf{K}$ points of a QD-SL Brillouin zone to be done at several points at the cost of the single QD calculation at each point $\mathbf{K}$, avoiding laborious calculations of the large QD clusters. All the results presented here were obtained by using the KPPW code.[46,47]

III. ELECTRONIC AND ABSORPTION CHARACTERISTICS OF QD ARRAY

A. Model QD arrays

The model QD arrays considered here consists of InAs/GaAs QDs with truncated pyramidal shape. The size and shape of the QD is controlled by the pyramid base length, b, its height h, and truncation factor, t, defined as a ratio between length of the pyramid side at h and length of the pyramid base b. The QDs are embedded in the tetragonal-like unit cell, $\Omega = L_x \times L_y \times L_z$. The vertical periodicity of the QD array is controlled by $L_z = d_z + h + L_{\mathrm{WL}}$, where d_z is the vertical separation of the QDs in subsequent layers, i.e., the distance between the top of the QDs and the bottom of the wetting layer (WL) in the following layer. The d_z is varied with $L_x = L_y$ chosen to be large enough to prevent lateral electronic coupling. All the results present in this paper are obtained at the single-particle level of theory.

B. Wave-function delocalization and intermediate-band formation in QD arrays

The origin of the intermediate-band formation in the QD arrays lays in the electronic coupling of states in neighboring QDs. When QDs are put close enough, the QD states eventually become delocalized over QDs in an array. By varying the QD size and vertical spacing between them it is possible to control electronic properties of the QD array. In Fig. 2, the evolution of QD states delocalization, "bonding," is shown. In Fig. 2(a) the charge densities of the electron ground (e_0) and first excited (e_1) states in CB and the hole ground (h_0) and first excited (h_1) states in VB of a single isolated InAs/GaAs QD with $b=10$ nm, $h=2.5$ nm, and truncation factor $t=0.5$ (which means that the side of the pyramidal shaped QD at $h=2.5$ nm is 5 nm) is shown. It can be seen that for such a QD all considered states are well-localized inside the QD. Once QDs are put in an array structure, the wave functions start to delocalize. In Figs. 2(b) and 2(c) the same size QD as in Fig. 2(a) are used and put in an infinite periodic array with vertical spacing between the QDs of $d_z=3$ nm and $d_z=2$ nm, respectively. It is clear that closer packing of QDs enhances the wave-function delocalization. This wave-function delocalization is the main cause of *intermediate-band formation* in QD array.

In analogy with solid-state physics, from Fig. 2(b), one can quantify the character of bonding of QD states in an InAs/GaAs QD array as *covalent* rather than *metallic*. The wave functions are delocalized only to some degree with charge density in the barrier region between QDs hardly ex-

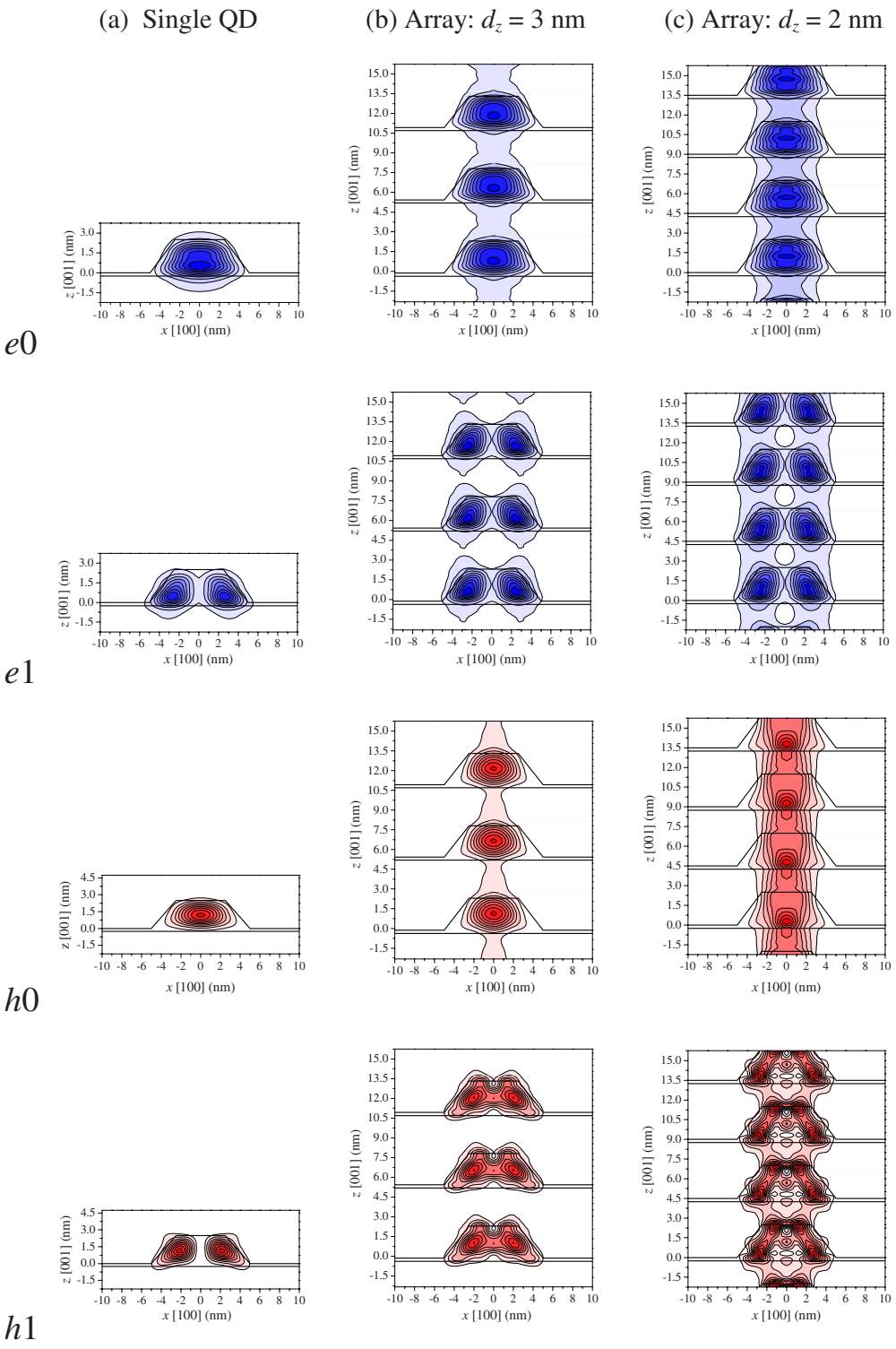

FIG. 2. (Color online) Evolution of the QD wave-functions delocalization in QD array as a function of the vertical proximity of QD in an array. The InAs/GaAs QD is with b=10 nm, h=2.5 nm, and truncation factor is t=0.5. (a) Single QD structure, (b) QD array with vertical spacer distance d_z=3 nm, and (c) QD array with vertical spacer distance d_z=2 nm.

ceeding 20% of its maximal value and are far from being completely delocalized to result in nearly free-electron motion in z direction, unlike the situation in quantum wires (QWRs). This is mainly due to strong carrier confinement imposed by InAs/GaAs QDs potentials in CB and VB.

C. Electronic structure of QD arrays

When a large number of identical QDs are brought together to form a QD array, the number of wave functions becomes exceedingly large (infinite for an infinite array), and

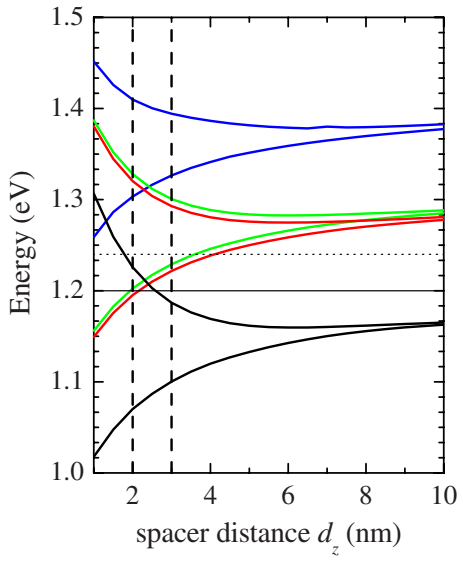

FIG. 3. (Color online) Variation in the first four, optically strongest, minibands width in the CB with the QDs vertical spacing. The two vertical lines correspond to values of the vertical spacing of $d_z=2$ nm and $d_z=3$ nm. Two horizontal lines corresponds to: the fully relaxed CB edge of the barrier GaAs material away for the QD (solid line) and highest point in the strain-induced CB "wing" at the interface between QD and barrier material (dotted line). Reference zero energy is taken at the top of the unstrained valence band of the QD material.

the difference in energy between them becomes very small (infinitesimal), so the levels may be considered to form continuous bands of energy rather than the discrete energy levels of the QD in isolation.[53] New normalized solution inside continuous bands of an QD array can be rewritten in the form of QD array Bloch states, $\propto e^{iK_z z}$, where the QD *array wave number*, K_z, is chosen within range $-\pi/L_z \leq K_z \leq \pi/L_z$. This range of the QD array wave numbers form the QD array BZ. However, some intervals of energy contain no wave functions, no matter how many QD are aggregated, forming energy gaps. Those energy gaps are between intermediate bands and not to be confused with energy gap of the underlying QD or barrier constituent materials. They will be referred later as a region of pure zero density of states (DOS) inside CB that fundamentally distinguishes the properties of a QD array structure from those of QWRs and are one of key factors for successful operation of the IBSC. Those regions (gaps) of pure zero DOS can prevent rapid thermal depopulation of carriers from higher states in QD array's CB to IB originated from delocalized ground states (e_0).

To estimate the variation in the first few minibands (i.e., intermediate bands) with the vertical periodicity of the QD array, in Fig. 3, we have changed the vertical spacing, d_z between QD array layers in the range from 1 to 10 nm (note that this is the distance between bottom of the WL in $(i+1)$th and top of the QDs in the ith growth layer). The lower and upper boundaries of an IB correspond to $K_z=0$ and $K_z=\pi/L_z$, respectively. The width of the e_0 miniband at the close spacing of $d_z=2$ nm is: 156 meV, at $d_z=3$ nm is: 86 meV, at $d_z=5$ nm is: 29 meV, and almost vanishes by $d_z=10$ nm. At the technologically feasible distance of $d_z=10$ nm the width of the e_0 miniband is $<10^{-6}$ eV. While the energy gap between VB and CB states exists both in bulk and nanostructured semiconductor materials (like in quantum wells, quantum wires, and quantum dots), one of the main reasons for using QD arrays for IBSC is to open another energy gap, the gap between e_0 miniband induced by QD array, i.e., IB, and the rest of the CB spectra. In the QD arrays consisting of small size QDs, suggested as desirable combination for the IBSC,[41] the e_1 and e_2 minibands are very close to or even overlap with the CB edge of the barrier material. In this case the IB-CB energy gap can be quantified as the energy difference between the lower boundary of the e_1 miniband that corresponds to $K_z=0$ and the upper boundary of e_0 miniband that corresponds to $K_z=\pi/L_z$. The IB-CB energy gap does not exists for the QDs closely spaced below some critical vertical distance $d_z^{(c)}$. This distance can be determined from the crossing point between the lower e_1 miniband and the upper e_0 miniband boundaries, i.e., from the condition $E_{e_1}(K_z=0)=E_{e_0}(K_z=\pi/L_z)$. In our case the region of zero IB-CB energy gap occurs for $d_z<2.4$ nm. In this region the QD arrays effectively exhibit electronic properties of a QWR structure with electron-free motion allowed in the z direction. As can be seen in Fig. 2(c) at $d_z=2$ nm the wave-function delocalization is substantial and form almost "metallic" like bonds. For larger vertical distances, e.g., $d_z=3$ nm, the IB-CB energy gap is 35 meV, while for $d_z=5$ nm this gap increases to 88 meV. Although this value is much lower than optimal one, of $\sim$700 meV, obtained under idealized assumptions,[5] it still proves the concept of realizing IB using QD arrays. The evolution of minibands broadening in the CB together with profile of the CB edge of strained InAs QDs inside GaAs barrier material along z direction and for $(x,y)=(0,0)$ is shown in Fig. 4. Due to the choice of QD (that has discrete δ function like nature of the DOS as an artificial atom[54]) as a building block of the QD array, the energy gaps between IBs in the conduction band are also characterized by pure zero DOS. To distinguish the regions where QD array behaves effectively as a QWR from the one suitable for IBSC application, in Fig. 5 the DOS of QD arrays is presented for two vertical spacer distances: (a) $d_z=2$ nm and (b) $d_z=5$ nm. In Fig. 5(b) one can clearly recognize pure zero DOS regions between minibands while such regions do not exist in Fig. 5(a). Furthermore, sharp peaks at the edges of minibands correspond to van Hove singularities of the DOS at the critical points of the QD-array Brillouin zone, i.e., at Γ and X points.

An alternative way of designing the electronic structure of the QD arrays for IBSC is to change QD sizes in the arrays.[41]

D. Absorption characteristics of QD arrays

As shown schematically in Fig. 1, the rationale for using IBSCs as absorbing material is to create a partially occupied IB, thus affording subband-gap absorption VB→IB into the empty states of the IB (process 2) and IB→CB from the occupied states of IB (process 3) in addition to the VB→CB of the host absorbing material (process 1). A few conditions have to be met for achieving good efficiency within such a concept.[55] (i) The VB→IB and IB→CB absorption

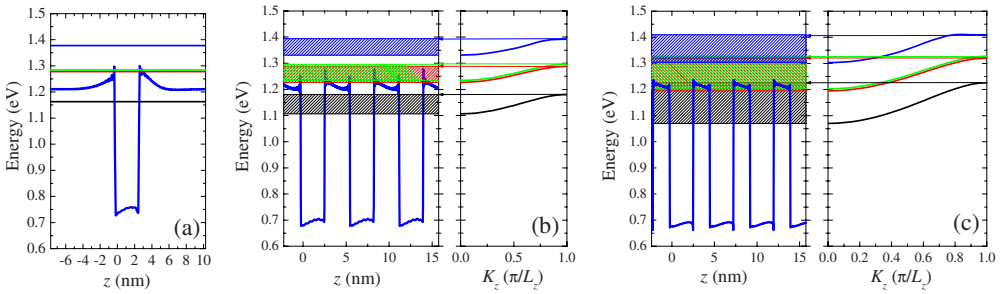

FIG. 4. (Color online) Conduction-band edge profile, along the z direction and $(x,y)=(0,0)$, of the QD/QD array, for: (a) single QD; (b) QD array made of the same QD as in (a) vertically spaced by $d_z=3$ nm; and (c) QD array made of the same QD as in (a) vertically spaced by $d_z=2$ nm. For QD arrays in (b) and (c) the dispersion of the first four, optically strongest, states in CB in the direction of the QD array is also shown. For QD array in (b) the energy gap between intermediate band e_0 and intermediate band e_1 can be identified while this gap disappears for closely spaced QD in array (c).

spectra should ideally have no spectral overlap. As we have shown in Sec. III C this condition can be achieved by designing the QD array with pure zero DOS between IB band and the rest of the CB electronic structure. This "photon-sorting" condition ensures maximum quantum efficiency for given positions of the CB-IB energy gap E_{gL} and IB-VB energy gap E_{gH} in Fig. 1. (ii) The VB $\rightarrow$ IB and IB $\rightarrow$ CB excitations must be optically allowed and strong. Thus, the quantum objects creating the IB must have significant concentration and oscillator strength.

The optical matrix element required for description of absorption and radiative related processes is defined as $|\hat{\mathbf{e}}\cdot\mathbf{p}_{if}|^2$, where $\hat{\mathbf{e}}$ is the unity light polarization vector and $\mathbf{p}_{if}(\mathbf{k})=(m_0/\hbar)\langle i|\partial H_{\mathbf{k}}/\partial\mathbf{k}|f\rangle$ is the electron-hole momentum operator of the quantum structure, where $|i\rangle$ and $|f\rangle$ are initial and final states involved in the process. In the QD array structure $\mathbf{k}\rightarrow\mathbf{k}+\mathbf{K}$. From the $\mathbf{K}$-dependent electronic structure, defined in Sec. III C, and momentum matrix element $\mathbf{p}_{ij}(\mathbf{K})$ the absorption coefficient, of the QD array were calculated (defined as a number of photons absorbed per unit volume per second divided by a total number of photons injected per unit area per second; and given in the units of cm^{-1}), in the dipole approximation

$$\alpha(\hbar\omega)=\frac{\pi e^2}{c\epsilon_0 m_0^2\bar{n}\omega b^2}\sum_{i,f,\mathbf{K}} f_{if}(\hbar\omega,\mathbf{K})(f_i-f_f), \tag{7}$$

where we define the *transition strength* as

$$f_{if}(\hbar\omega,\mathbf{K})=|\hat{\mathbf{e}}\cdot\mathbf{p}_{if}(\mathbf{K})|^2\delta[E_i(\mathbf{K})-E_f(\mathbf{K})-\hbar\omega] \tag{8}$$

and e is the electron charge, c is the speed of light in vacuum, m_0 is the rest electron mass, $\bar{n}$ is the refractive index of the GaAs, ϵ_0 is the vacuum permittivity, ω is the light frequency, b^2 is the area of the QDs base, and f_i and f_f are the Fermi distributions for the initial and final miniband, respectively. The delta function, $\delta[x]$, is replaced with a Gaussian function $\exp[-(x/\sqrt{2}\sigma)^2]/(\sqrt{2\pi}\sigma)$, defined by the phenomenological broadening σ, to take into account random fluctuations in the structure of the QD array. Finally, the summation is replaced by integration over the wave vector K_z. The choice of the absorbing area in Eq. (7) is somewhat arbitrary. Although we have chosen this area to be equal to the base of QDs in the array, $(1/b^2)$, it would probably be closer to experimentally observed values if this factor is chosen to be proportional to the surface density of QDs, $(1/A)$, i.e., QD coverage fraction. The value of QD array absorption coefficient, that would take the QD coverage fraction instead, can be easily obtained for the Eq. (7) by simple multiplication with the factor b^2/A. Absorption coefficient given in terms of the QD coverage fraction is always smaller than that obtained by Eq. (7).

Assuming the IB formed by the QD-array miniband originated from the ground state e_0 and separated by zero DOS from the rest of the CB spectra, the IB $\rightarrow$ CB and VB $\rightarrow$ IB involve e_0 as initial and final miniband, respectively. Due to a finite width of the e_0 miniband, in our IBSC absorption

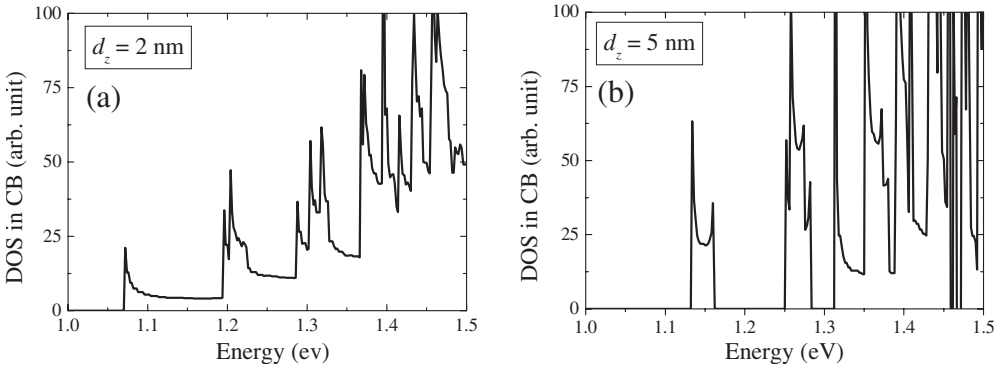

FIG. 5. Density of states in the conduction band for QD array with vertical periodicity (left) $d_z=2$ nm and (right) $d_z=5$ nm.

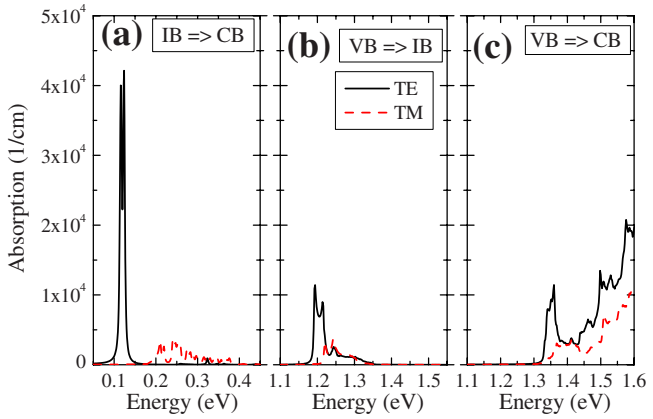

FIG. 6. (Color online) Absorption spectra of QD array with vertical periodicity $d_z=5$ nm. (a) IB→CB absorption, (b) VB →IB absorption, and (c) VB→CB absorption. Both the TE (solid line) and TM (dashed line) polarizations are presented.

model, we can introduce an approximation that the final miniband states involved in the particular absorption process are always empty, i.e., $f_f=0$. The corresponding absorption coefficients $\alpha^{\mathrm{VB}\to\mathrm{IB}}(\hbar\omega)$, $\alpha^{\mathrm{IB}\to\mathrm{CB}}(\hbar\omega)$, and $\alpha^{\mathrm{VB}\to\mathrm{CB}}(\hbar\omega)$ are then calculated taking into account 1000 hole minibands in the VB and the e_0 miniband as the IB, the e_0 miniband as the IB and the next 100 minbands in the CB starting from e_1 miniband, and using 1000 hole minibands in the VB and 100 minbands in the CB starting from e_1 miniband, respectively.

Figure 6 shows all relevant absorption coefficients of the QD array made of truncated pyramidal InAs/GaAs QDs with $b=10$ nm, $h=2.5$ nm, and $t=0.5$, and with vertical spacing between the dots in the array of $d_z=5$ nm. First in Fig. 6(a) the transitions from QD array CB ground-state e_0 miniband to all other electron minibands higher in energy are presented. A sharp double peak that appears at 0.117 and 0.125 eV (full width at half maximum=14 meV) corresponds to all the momentum-allowed transitions between e_0 and e_1, e_2 minibands. This IB→CB absorption peak is completely TE polarized[56] due to S symmetry of the QD states forming e_0 miniband and $P_{x,y}$ symmetry of the QD states forming e_1 and e_2 minibands. It should be emphasized that e_1 and e_2 minibands are already overlapped with the conduction-band minima (CBM) of the barrier material. Existence of the pronounced peaks at ~0.117–0.124 eV suggests that the condition (ii) that IB→CB excitations must be optically allowed and strong, can be fulfilled by relatively small $b=10$ nm, InAs/GaAs QDs vertically stacked with $d_z=5$ nm in the QD array. Further above the barrier CBM, in the energy range of 0.2–0.4 eV, a spectra of weak TE-polarized transitions can be seen. This part of the IB→CB absorption spectra corresponds to transitions between e_0 miniband and largely delocalized states between QDs. The second absorption process relevant for IBSC operation is associated to the VB→IB transitions. This absorption coefficient has been calculated again using Eq. (7) with the first electron miniband e_0 taken now as final and unoccupied. As initial minibands we considered the first 1000 hole minibands starting from h_0 miniband. The lowest energy of the 1000th hole miniband goes well below the valence-band maximum (VBM) in the barrier material. The calculated absorption coefficient of VB→IB process is shown in Fig. 6(b). The absorption peak is at ~1.2 eV and again of the TE polarization. This time the TE polarization originates from heavy-hole QDs states that have no admixture of the orbital of the underlying bulk material with P_z symmetry. Due to highly strained InAs QD material in GaAs matrix, the biaxial component of the compressive strain splits the heavy from light hole states in the VB while hydrostatic component of the strain pushes heavy-hole states upward on the absolute energy scale making h_0 miniband of heavy-hole character. The shoulder in the absorption spectra between 1.23 and 1.35 eV corresponds to transitions between deep VB minibands and e_0 miniband. The third absorption process, VB→CB, is shown in Fig. 6(c). This absorption spectra was obtained using first 1000 minibands in the VB as initial states and 100 empty minibands in the CB starting from e_1 miniband as final states. The absorption edge for this process is at 1.33 eV and is determined by energy distance between h_0 and e_1 minibands.

As mentioned in Sec. III A, all the presented results are obtained at the single-particle level of theory. In the presence of Coulomb interaction, however, in GaAs bulk there exists a continuum of "free-carrier" excitons where Coulomb interaction enhances the joint electron-hole density of states. The measure of this enhancement is given by the Sommerfeld factor,[57,58] which for allowed transitions in the bulk material was obtained as $S=\pi\alpha_3 e^{\pi\alpha_3}/\sinh\pi\alpha_3$, where $\alpha_3=[\mathrm{Ry}^*/(E-E_g^{\mathrm{GaAs}})]^{1/2}$ and $\mathrm{Ry}^*=(\mu^*/m_0\epsilon_r)\mathrm{Ry}$ is the effective Rydberg constant, $1/\mu^*=1/m_e^*+1/m_h^*$ is the reduced effective mass of the electron-hole pair, ϵ_r is the dielectric constant of GaAs, and Ry=13.6 eV. Although the Sommerfeld factor, S, is always larger than unity, indicating that the Coulomb attraction between an electron and a hole enhances the optical absorption in the bulk material, it should also be noticed that S is large near the band edge but tends to unity at higher energies. In bulk GaAs, $\mathrm{Ry}^*\approx 5$ meV, which means that the excitons are nearly always ionized at the room temperature, and hence are not important in the barrier bulk material. At low temperatures, however, they can contribute to the absorption spectra with near edge peak of $\alpha\simeq 10^4$ 1/cm,[59] that would be comparable to the first peak (at ~1.35 eV) in the VB →CB spectra in Fig. 6(c).

The intensity of the VB→IB and VB→CB absorption peaks are roughly the same, $\sim 10^4$ cm^{-1}, while IB→CB peak is four times larger despite the fact that the large portion of e_1 and e_2 minibands being above the GaAs barrier CBM. It suggests a strong, by QD periodicity induced, *Bragg-type confinement* of states in e_1 and e_2 minibands that are predominantly confined above the barrier in the continuum.[60,61] Those states partly overlap with CBM while the rest of those minibands are above CBM as can be seen in Fig. 4(c).

It has been shown previously that using larger QDs (b ~20 nm) in the QD array the bulklike absorption spectra can only be "redshifted" by almost continuum spectra of electron and hole minibands while distinct absorption peak associated with IB cannot be identified.[41,62]

IV. RADIATIVE AND NONRADIATIVE PROCESSES IN QD ARRAY

Apart from the requirements related to photon-sorting, strong absorption, and request to design suitable material that

can provide E_{gL}=0.7 eV, E_{gH}=1.2 eV, and E_g=1.9 eV, that will ultimately lead to maximal efficiency of the IBSC under concentrated light, there are a number of possible deleterious effects related to carrier lifetimes, that can affect carrier transport in IBSC, and need to be minimized. In the following sections we will discuss radiative relaxation times between CB→IB and IB→VB in QD array and only those nonradiative times that perhaps might compete with radiative once: (i) longitudinal-optical phonon scattering between the CB and IB states and (ii) Auger-related nonradiative scattering times between states in CB and IB, *electron cooling* process, and Auger *biexcitonic recombination* that occurs between carriers in IB and VB.

A. Radiative processes in QD arrays

The *radiative recombination* is an unavoidable process in direct gap semiconductor materials that causes loss of free electrons and holes from the transport process. It is a spontaneous process defined as the transition probability of an electron from initial state $|i\rangle$ to the final state $|f\rangle$ that is followed by photon emission of frequency $\omega=(E_i-E_f)/\hbar$. The radiative recombination defines the ultimate efficiency of the SC which is also referred to as *radiative limit* efficiency.

Starting from Fermi's golden rule and assuming the wavelength of the sunlight much larger than the size of the QD array with which it interacts (i.e., in the dipole approximation),[63–65] the expression for the radiative recombination in the QD array is

$$\frac{1}{\tau_{if}^{\mathrm{rad}}(\mathbf{K})}=\frac{4}{3}\frac{\bar{n}[E_i(\mathbf{K})-E_f(\mathbf{K})]}{\pi\hbar^2c^3\epsilon_0}[|\hat{e}_x\cdot\mathbf{p}_{if}(\mathbf{K})|^2+|\hat{e}_y\cdot\mathbf{p}_{if}(\mathbf{K})|^2+|\hat{e}_z\cdot\mathbf{p}_{if}(\mathbf{K})|^2], \quad (9)$$

where, c is the speed of light in vacuum, $\bar{n}$ is the refractive index of the GaAs, and ϵ_0 is the vacuum permittivity. Since the radiative lifetime, τ_{if}^{rad}, is determined mainly by the momentum matrix element $\mathbf{p}_{if}(\mathbf{K})$ and energy difference between initial and finale states, $E_i(\mathbf{K})-E_f(\mathbf{K})$, the quantum nanostructures design can offer extra degree of freedom in modifying the value of this scattering time.

In Fig. 7 the variation in the radiative transition time across the BZ of QD array, between e_1, e_2 minibands (CB) and e_0 miniband (IB) and between e_0 miniband (IB) and h_0 miniband (VB) is shown. In a single InAs/GaAs QD, (b,h) =(10,2.5) nm, the radiative lifetime between electron and hole ground state is $\tau_{e_0,h_0}^{\mathrm{rad}}=1.59$ ns. When the same size QD form an array, at the K_z=0 edge, the radiative time is $\tau_{\mathrm{IB}(e_0),\mathrm{VB}(h_0)}^{\mathrm{rad}}(K_z=0)=2.1$ ns. The increase in the radiative relaxation time of 32% in QD array when compared to single QD is explained in terms of e_0 and h_0 wave-function delocalization in QD array due to electronic states coupling from neighboring QDs. Wave-function delocalization reduces the value of the momentum matrix element which, in turn, increases the value of τ^{rad}.

In the single QD structure the $\tau_{e_1,e_0}^{\mathrm{rad}}=149$ ns and $\tau_{e_2,e_0}^{\mathrm{rad}}$ =129 ns. Although, one might expect that e_0 miniband states, already shown to be delocalized by close proximity of QDs in the QD array, will further increase the values of

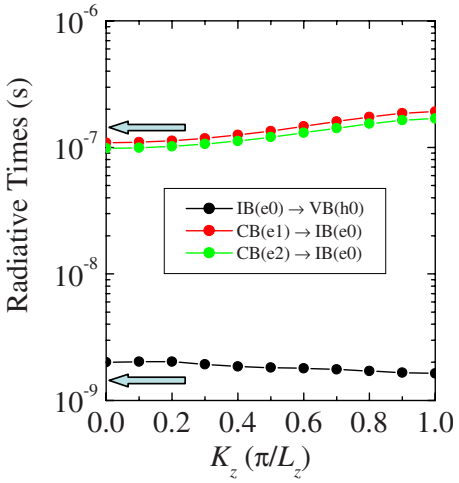

FIG. 7. (Color online) Variation in the radiative transition times between CB(e_2) and IB(e_0); CB(e_1) and IB(e_0) that can be regarded as CB to IB radiative processes, and between IB(e_0) and VB(h_0) that can be regarded as IB to VB radiative process. Horizontal arrows mark the equivalent single QD radiative times.

radiative times $\tau_{\mathrm{CB}(e_1),\mathrm{IB}(e_0)}^{\mathrm{rad}}$ and $\tau_{\mathrm{CB}(e_2),\mathrm{IB}(e_0)}^{\mathrm{rad}}$, in the QD array structure the trend is indeed opposite. The radiative transition times between states in two minibands e_1 and e_2 that overlap with the CBM edge of barrier material and the e_0 miniband regarded as an IB, at the K_z=0 edge, are $\tau_{\mathrm{CB}(e_1),\mathrm{IB}(e_0)}^{\mathrm{rad}}(K_z=0)=109$ ns and $\tau_{\mathrm{CB}(e_1),\mathrm{IB}(e_0)}^{\mathrm{rad}}(K_z=0)=98$ ns and are smaller than for the equivalent radiative transitions in single QD. This trend supports the idea of the QD array-induced Bragg-type confinement of e_1 and e_2 miniband states. Those states overlap or are only just above the CBM edge of the barrier material and should not be confused with the strain-induced confinement at the QD/barrier surfaces of the QD.[66]

It should be mentioned that $\tau_{\mathrm{CB}(e_1,e_2),\mathrm{IB}(e_0)}^{\mathrm{rad}}$ are intersubband transitions inside CB with energy difference in the range of ~100 meV while $\tau_{\mathrm{IB}(e_0),\mathrm{VB}(h_0)}^{\mathrm{rad}}$ is intraband transition between states in CB and VB with energy difference of ~1 eV. This discrepancy in transition energies causes the big difference in radiative relaxation times, $\tau_{\mathrm{CB,IB}}^{\mathrm{rad}}/\tau_{\mathrm{IB,VB}}^{\mathrm{rad}}$ ~52, between CB→IB and IB→VB transitions.

The radiative recombination is the detailed balance counterpart of the corresponding rate of electron-hole pair generation by thermal radiation.[67] Therefore, if the transition strength is large the radiative recombination is strong and the radiative lifetime small. To compare the radiative recombination between different transitions, $|a\rangle\rightarrow|b\rangle$ and $|c\rangle\rightarrow|d\rangle$, not only the transition strength but the transition energy too needs to be taken into account. In the Appendix A we have shown that radiative lifetime follows the trend of the transition strength as defined in Eq. (8) and relate this to the absorption coefficient of the QD array.

B. Auger-related nonradiative times in QD arrays

Nonradiative Auger-related scattering processes play an important role in carrier dynamics in semiconductor nanostructures when both types of carriers (electrons and holes)

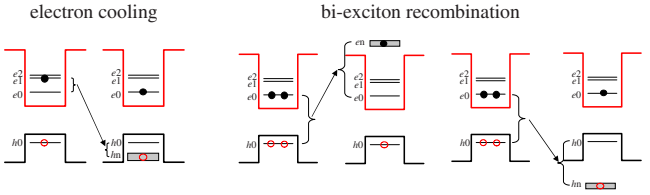

FIG. 8. (Color online) Illustration of two different Auger processes: electron cooling (left) and biexciton recombination (right).

are present. They become significant particularly in QDs which have discrete electronic levels, which implies that the other nonradiative competing processes (like phonon scattering) could be strongly suppressed.[68] We consider two main Auger-related nonradiative processes: *electron cooling* and *biexciton recombination* (Fig. 8) as they might compete on the time scale with its radiative recombination counterparts, $\tau^{\mathrm{rad}}_{\mathrm{CB,IB}}$ and $\tau^{\mathrm{rad}}_{\mathrm{IB,VB}}$, respectively. We adopt a phenomenological formula for the Auger rate derived under the standard time-dependent perturbation theory and using Fermi's golden rule[69,70]

$$\frac{1}{\tau^{\mathrm{A}}_{if_n}} = \frac{2\pi}{\hbar}\sum_n |J(i,j;k,l)|^2 \delta(\Delta E + E_{f_n} - E_i), \tag{10}$$

where the Coulomb integral is defined as

$$J(i,j;k,l) = \frac{1}{4\pi\epsilon_0\epsilon_r}\int d\mathbf{r}_1 \int d\mathbf{r}_2 \frac{\psi_i^*(\mathbf{r}_1,s_1)\psi_j^*(\mathbf{r}_2,s_2)\psi_k(\mathbf{r}_1,s_1)\psi_l(\mathbf{r}_2,s_2)}{|\mathbf{r}_1-\mathbf{r}_2|} \tag{11}$$

and $\{\psi_i\}$ are the single-particle wave functions and $s_{1,2}$ are the electron-spin state (up or down). In Eq. (10) the i and f_n are initial and final electronic configurations involved in a particular Auger process, E_i and E_{f_n} are their energies, and ΔE is the energy transfer between initial and final configurations. In Eq. (10), we have used multiple final states f_n (where n includes spin as well), since each final state might have some contributions to the Auger rate. As in the case of absorption spectra, δ function is replaced by a Gaussian function $\exp[-(x/\sqrt{2}\sigma)^2]/(\sqrt{2\pi}\sigma)$, defined by the phenomenological broadening σ, to take into account inhomogeneous line broadening due to size-distribution effects as well as homogeneous line broadening. To achieve convergence of our results, the number of final states used, in particular, Auger process is determined from the condition that $|\max\{E_{f_n}\}-\min\{E_{f_n}\}|/2 \geq 2\sigma$, i.e., to be inside two standard deviations and $\sigma=5$ meV.

In the electron-cooling process, in which one electron is initially in e_1 state and hole is in its ground state h_0, the energy transfer occurs when electron relaxes to its ground state e_0 to transfer excess energy $\Delta E=E_{e_1}-E_{e_0}$ to the hole in order to excite it by ΔE deeper into VB. The Coulomb integral in Eq. (10) reads as $J(h_0,e_1;h_n,e_0)$. We have estimated that the Auger electron cooling in single InAs/GaAs QD is $\tau^{\mathrm{A}}_{\mathrm{e\text{-}cool}}=1.37$ ps (excitonic gap 1.13 eV) which is in very good agreement with other theoretical and experimental results.[70–72] In QD array the electron cooling time is increased to $\tau^{\mathrm{A}}_{\mathrm{e\text{-}cool}}=2.05$ ps, despite further decrease in the excitonic gap to 1.09 eV. The main reason for this increase is delocalization of states involved in the process and long-range Coulomb interaction between charges in neighboring QDs in the array that was compensated in a single QD structure by Makov-Payne correction.[47,73]

In the biexiciton Auger relaxation one exciton, composed of electron and hole in their ground states, recombines while the energy, $\Delta E=E_{\mathrm{X}}$, released in this process is transferred to the other electron (hole) in the ground state (with opposite spin) to be excited to the states higher (lower) in CB (VB) by ΔE. These two processes are denoted as $\tau^{\mathrm{A}}_{e,\mathrm{ex}}$ and $\tau^{\mathrm{A}}_{h,\mathrm{ex}}$ while Coulomb integrals in Eq. (10) takes the form $J(e_{0,\alpha},e_{0,\beta};e_n,h_0)-J(e_{0,\beta},e_{0,\alpha};e_n,h_0)$ and $J(h_{0,\alpha},h_{0,\beta};h_n,e_0)-J(h_{0,\beta},h_{0,\alpha};h_n,e_0)$, respectively, where α and β stands for opposite spins. The biexciton recombination time is then: $1/\tau^{\mathrm{A}}_{\mathrm{bx}}=2/\tau^{\mathrm{A}}_{e,\mathrm{ex}}+2/\tau^{\mathrm{A}}_{h,\mathrm{ex}}$. Unlike in colloidal QD structures,[69] in our InAs/GaAs QD array system the final configuration involves highly delocalized electron (hole) states located above (below) conduction- (valence-) band edge of the barrier GaAs material, Fig. 8. In a single InAs/GaAs QD considered here we estimated: $\tau^{\mathrm{A}}_{e,\mathrm{ex}}=209$ ns, $\tau^{\mathrm{A}}_{h,\mathrm{ex}}=6.15$ ns, and $\tau^{\mathrm{A}}_{\mathrm{bx}}=3$ ns while for InAs/GaAs QD array made of the same size QDs: $\tau^{\mathrm{A}}_{e,\mathrm{ex}}=266$ ns, $\tau^{\mathrm{A}}_{h,\mathrm{ex}}=18$ ns, and $\tau^{\mathrm{A}}_{\mathrm{bx}}=8.4$ ns. A similar Auger times ($\sim>10$ nm), related to e_0-h_0 transition, were reported in the literature for the InAs QDs.[74,75] The trend that $\tau^{\mathrm{A}}_{e,\mathrm{ex}} \gg \tau^{\mathrm{A}}_{h,\mathrm{ex}}$ was already observed in semiconductor quantum-well structures both experimentally and theoretically.[76–78]

The results concerning Auger lifetimes are presented at the single particles level of theory without full treatment of any other existing electrons or holes, "spectators," in the system.[69] Due to the presence of other electrons or holes, and after proper configuration interaction (CI) treatment of the correlation and exchange interaction with already existing particles involved in the Auger cooling process, the Auger cooling time is likely to increase. For the colloidal CdSe QD, which have very high offsets in the conduction and valence bands that can provide a very good confinement of many electron and hole states, it was shown that this increase is about $\sim$1–2 orders of magnitude, compared to Auger cooling time estimated at the single-electron level of theory.[69] However, in InAs/GaAs QDs system, with much weaker state confinement than in CdSe QDs, the effect of correlation and exchange can only be less pronounced. If we compare the magnitude of the excitonic shift (i.e., e_0-h_0 Coulomb interaction energy) in the two cases: few hundreds of millielectron volt in the case of CdSe QD,[69] vs few tens of millielectron volt in InAs/GaAs QDs;[39,40,47] one cannot expect that the presence of a spectator exciton has an effect of the same magnitude in the two systems. We expect the increase in InAs/GaAs QDs to be of the same order of magnitude as single-particle lifetime, i.e., on the order of 1–2 ps.[79] Even if Auger cooling time, between e_1 and e_0, in the presence of other charged particles in the system increases by 2 orders of magnitude, it will still be $\sim$1000 times faster than radiative transition time between those two states.

In the Auger biexciton recombination process, although the carriers are excited to levels in the continuum, above the

potential well of the QD, the localized QD levels must each, because of quantization, be described using a range of wave vectors. This leads to a breakdown in all three directions of the strict **k**-selection rule which restricts Auger recombination in bulk semiconductors. This process can also be affected by the presence of other charges in the system and correlations between them. As mentioned above, the Coulomb interaction between charges in the InAs/GaAs QD confined states are on the order of few tens of millielectron volt and from this argument alone it is unlikely that this will change Auger biexciton recombination dramatically. The correlation effects will tend to reduce the excitonic energy gap $E^{\mathrm{X}}_{e_0,h_0} < \Delta E_{e_0,h_0} = E_{e_0} - E_{h_0}$. After energy transfer of $\Delta E = E^{\mathrm{X}}_{e_0,h_0}$ to another electron (hole), they will be promoted into the GaAs continuum, in the region with smaller density of states than if no correlations were included, i.e., if $\Delta E = \Delta E_{e_0,h_0}$.[80] This, in turn, will slightly increase $\tau^{\mathrm{A}}_{\mathrm{bx}}$. However, it is quite tricky to guess what may happen, as the final states would all be different from the single-particles case, due to the energy shift one would get with full many-body treatment. As discussed above the Coulomb interaction enhances the joint electron-hole "free-carrier" exciton density of states. It is still an open question how much this joint density of states is increased at the energy ~1 eV above the GaAs band gap at temperatures relevant for the operation of the IBSC?

Certainly, to safely resolve the issues of the many-body effects and their influence on the Auger recombination, a more elaborate theory is required. Such theory should be based either on the large CI method or Feynman path-integral formulations.[81]

C. Electron-phonon interaction in QD arrays

At finite temperatures atoms in crystal can vibrate around their equilibrium positions. These lattice vibrations are quantized and are called *phonons*. Phonons create additional potential that perturbs otherwise stationary electronic states and causes transitions between them. Here, only the polar coupling to optical phonons will be considered because other types of phonon interactions are much weaker or irrelevant in the QD-based systems.[82] The Frölich interaction Hamiltonian describing polar coupling to optical phonons is given by[83]

$$\hat{\mathrm{H}}_{\text{e-ph}} = \sum_{i,f,\mathbf{q}} \alpha(\mathbf{q}) F_{if}(\mathbf{q}) \hat{a}_i^{\dagger} \hat{a}_f (\hat{b}_{\mathbf{q}} + \hat{b}_{-\mathbf{q}}^{\dagger}), \tag{12}$$

where $\mathbf{q}$ is the phonon wave vector, $\hat{b}_{\mathbf{q}}$ and $\hat{b}_{-\mathbf{q}}^{\dagger}$ are phonon annihilation and creation operators, $\hat{a}_i^{\dagger}$ and $\hat{a}_f$ are annihilation and creation operators for electrons. The factor $\alpha(\mathbf{q}) \propto q^{-1}\sqrt{\hbar\omega_{\mathrm{LO}}}$, and the form factor $F_{if}(\mathbf{q}) = \langle i | e^{i\mathbf{q}\cdot\mathbf{r}} | f \rangle / \sqrt{N}$, where N is the number of sampling points in the K_z space. It is assumed that an electron in initial state is always at the band edge while momentum conservation is achieved with $\mathbf{q} = \mathbf{k} + K_z \hat{z}$, i.e., phonon wave vector equals electron momentum in the final state. Optical phonons are nearly dispersionless, and for simplicity a constant LO phonon energy $\hbar\omega_{\mathrm{LO}} = 36$ meV is assumed.

In a single QD structure, due to the discrete nature of energy levels together with very weak-energy dispersion of the longitudinal-optical (LO) phonons, a simple consideration based on energy conservation only and Fermi's golden rule predicted that scattering rates are zero unless the electron level spacing equals the LO-phonon energy.[83] This largely reduced relaxation rate from the inefficient phonon scattering in QDs is referred in literature to as *phonon bottleneck*. This condition can be relaxed in QD array structures due to finite widths of minibands. Even so, such an approach treats the electron and phonon systems separately with their interaction being only a perturbation. It is currently known that electrons and phonons in quantum dots form coupled entities, *polarons*, and that the polaron lifetime is determined by anharmonic decay of an LO phonon into two low-energy bulk LA phonons.[84–87]

To describe that scattering mechanism, we follow a Wigner-Weisskopf description for the carrier relaxation in QD through LO-phonon scattering. If the electron couples directly to the LO-phonon modes, quantum transition would result in a repeated energy exchange between the electron and phonon modes, known also as Rabi oscillation. However, due to the decay of the confined LO phonons, this oscillation will decay rapidly, thus the electron energy is dissipated away through the LO phonons. With such assumptions, the polaron lifetime is given by[85]

$$\frac{1}{\tau^{\mathrm{LO}}_{if}} = W_{\mathrm{ph}} - \sqrt{2(R - X)}, \tag{13}$$

where $R = \sqrt{X^2 + Y^2}$ with $X = (g/\hbar)^2 + (\Delta_{if}^2 - W_{\mathrm{ph}}^2)/4$ and $Y = W_{\mathrm{ph}}\Delta_{if}/2$. Detuning from the phonon energy is $\Delta_{if} = E_i - E_f \mp \hbar\omega_{\mathrm{LO}}$ while W_{ph} is the phenomenological phonon decay rate due to LO phonon decay into two LA phonons and g is the coupling strength of an electron to all LO modes, which under the assumption of bulk LO-phonon modes and the Frölich interaction Hamiltonian reads

$$g^2 = \sum_{K_z'} \sum_{\mathbf{k}} \left(n_{\mathrm{LO}} + \frac{1}{2} \pm \frac{1}{2} \right) |\alpha(\mathbf{k})|^2 |F_{if}(\mathbf{k})|^2, \tag{14}$$

where n_{LO} is the phonon occupation number, and K_z' is the final state, $|f\rangle$ wave vector due to QD superlattice effect.[85,88] Since for the QD arrays with $d_z = 5$ nm the wave-function delocalization, due to effects of the array, is even weaker than in Fig. 2(b), we believe that the strong electron-phonon-coupling regime still holds. The above theoretical considerations have been verified by experimental results on intraband carrier dynamics in InAs/GaAs QDs vertically spaced for 50 nm.[87,89]

In Fig. 9, the LO phonon absorption (open dots) and emission (solid dots) scattering rates are presented between the first 100 states in the CB. It is clear that both processes exhibit sharp peaks for electron transitions energy in the vicinity of ± 36 meV which is the LO phonon energy. In this region electron-phonon scattering is on the order 10^{-9}–10^{-12} s. This energy region is not particularly important for operation of the IBSC. Indeed the fast phonon relaxation processes can help to prepare system in the state where electrons are in e_1 or e_2 miniband. At $K_z = 0$ the energy spac-

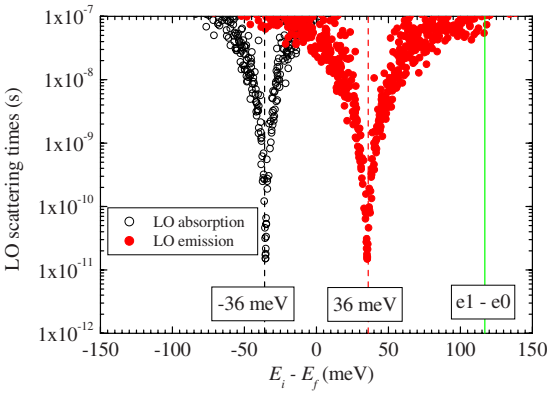

FIG. 9. (Color online) LO absorption and emission scattering times.

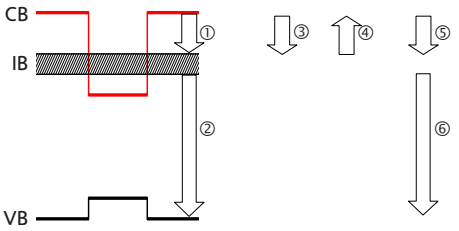

FIG. 10. (Color online) Schematic representation of radiative and nonradiative relaxation times in IBSC: (1) radiative recombination between CB and IB, (2) radiative recombination between IB and VB, (3) phonon-emission-assisted CB to IB relaxation, (4) phonon absorption assisted IB to CB scattering, (5) Auger electron cooling relaxation between CB and IB, and (6) Auger biexciton relaxation between IB and VB.

ing between e_1 miniband and IB originated from e_0 states is $\sim$117 meV. The LO phonon emission scattering time for this transition is $\tau^{\mathrm{LO(e)}}_{\mathrm{CB}(e_1),\mathrm{IB}(e_0)}=56$ ns, and it is increased for the QD array when compared to the same transition in the single QD which is $\tau^{\mathrm{LO(e)}}_{e_1,e_0}=19$ ns. Increase in this scattering time is attributed to decrease in both $F(\mathbf{q})$ form factor and Δ_{e_1,e_0} energy detuning factor in QD array. Compared to the radiative time $\tau^{\mathrm{rad}}_{\mathrm{CB}(e_1),\mathrm{IB}(e_0)}=109$ ns, the $\tau^{\mathrm{LO(e)}}_{\mathrm{CB}(e_1),\mathrm{IB}(e_0)}$ is somewhat smaller but still significantly larger than $\tau^{\mathrm{rad}}_{\mathrm{IB,VB}}=2.1$ ns, suggesting that nonradiative phonon-scattering-related processes between CB and IB might not be critical for operation of the IBSC based on QD array. Possible deteriorating effect of losing electrons from the IB, minband e_0, to the CB, miniband e_1 or e_2, is even less likely since phonon absorption process takes $\tau^{\mathrm{LO(a)}}_{\mathrm{IB}(e_0),\mathrm{CB}(e_1)}=650$ ns.

Acoustic phonon scattering is only significant when the states are closely spaced in energy ($<$10 meV). That is the case between higher miniband states in CB. For larger energy separation, like that between e_1 miniband and IB formed by e_0 state which is of the order $\sim$100 meV, the interaction with LO phonons is dominant.[63]

V. CONCLUSIONS

We have presented the comprehensive theoretical model for design and modeling of IBSC based on arrays of InAs/GaAs QDs. For one realistic QD array ($b=10$ nm, $h=2.5$ nm, $t=0.5$, and $d_z=5$ nm) we have estimated $E_{gH}=1.2$ eV and $E_{gL}=0.124$ eV. For these energies and absorption spectra found in Sec. III D we have estimated ultimate efficiency of the IBSC in the radiative limit to be $\eta\approx 39\%$ for undoped structure for sunlight concentration factor of 1000.[25] This is increase in 56% compared to simple QD solar cell.[90] Our finding suggests that with appropriate design of the QD array structural parameters: (i) it is possible to achieve the regions of pure zero DOS between IB and the rest of the CB states, that is desirable for photon sorting and increased efficiency of the device and (ii) it is possible to achieve the strong optically allowed excitation between IB and CB. Analysis of various radiative and nonradiative times summarized in Table I and schematically presented in Fig. 10 indicates that: (i) the ratio between CB$\rightarrow$IB and IB$\rightarrow$VB radiative times is $\sim$50, , (ii) nonradiative phonon absorption process that promotes electrons from IB to CB is very slow and probably would not significantly affect the transport properties of the IBSC, (iii) nonradiative phonon emission process that relax electrons from the CB to IB is about half time of the same radiative, CB$\rightarrow$IB, counterpart, and although faster it is still one order of magnitude slower than radiative IB$\rightarrow$VB process, and probably would not significantly affect transport either, (iv) nonradiative Auger biexciton relaxation time is longer then radiative IB to VB relaxation time, indicating that this process will still be predominantly radiative. This, however, needs to be taken with caution since other effects such as Coulomb correlations, QD shape variations, or size inhomogeneity can overcome this difference. (v) The most detrimental effect on transport properties can originate from nonradiatve Auger electron cooling process, that is in the picosecond timescale and is three orders of magnitude faster that any other relaxation process in the IBSC. Special attention needs to be paid in the design of the IBSC structures in order to suppress the effects of electron cooling and to provide an increased efficiency of the IBSCs. Possible material combination, that will reduce fast electron cooling, should consider Sb containing alloys for the barrier region in order to induce the type-II alignment and spatial electron/hole separation.

TABLE I. Radiative, LO-phonon emission/absorption, and Auger scattering times of InAs/GaAs QD array IBSC considered in the main text.

Type	Minibands	Radiative (ns)	Phonons [e/a] (ns)	Auger (ns)
CB$\rightarrow$IB	$e_1\rightarrow e_0$	109	56/650	2×10^{-3}
IB$\rightarrow$VB	$e_0\rightarrow h_0$	2.1		8.4

ACKNOWLEDGMENTS

The author wishes to thank to A. R. Adams FRS, M. Blake, M. Califano, N. M. Harrison, Z. Ikonić, T. S. Jones, A. Luque, A. Marti, E. P. O'Reilly, and N. Vukmirović for many useful discussions and suggestions. The author is

grateful to STFC Energy Strategy Initiative for financial support.

APPENDIX A: ABSORPTION COEFFICIENT AND RADIATIVE TRANSITION TIMES

According to the Fermi's Golden rule, the transition time, τ_{if}, from an initial state $|i\rangle$ to a final state $|f\rangle$ due to the spontaneous emission of photons (radiative lifetime) of angular frequency ω is given by

$$\frac{1}{\tau_{if}} = \frac{2\pi}{\hbar}\sum_{\mathbf{k}} |\langle i|H'_{\mathbf{k}}|f\rangle|^2 \delta(E_i - E_f - \hbar\omega), \tag{A1}$$

where E_i and E_f are the energies of the initial and final state, respectively. The Hamiltonian, $H'_{\mathbf{k}}$, of electron interaction with electromagnetic field is obtained by replacing $\mathbf{k}$ with $\mathbf{k}+(q/\hbar)\mathbf{A}$ in the kinetic part of the Hamiltonian, Eq. (4), (where $\mathbf{A}=A_0\hat{\mathbf{e}}$ is the magnetic vector potential), i.e., $H'_{\mathbf{k}} = H_{\mathbf{k}}[\mathbf{k}+(q/\hbar)\mathbf{A}] - H_{\mathbf{k}}[\mathbf{k}]$. In the dipole approximation $\mathbf{A}$ is considered constant in space, and all the terms quadratic in $\mathbf{A}$ are neglected. By substituting the expressions for $H'_{\mathbf{k}}$ and $\mathbf{A}$ into Eq. (A1), and after replacing summation over $\mathbf{k}$ vector with integration, i.e., $\Sigma_{\mathbf{k}} \rightarrow [\Omega/(2\pi)^3]\int d\mathbf{k}$ one gets

$$\frac{1}{\tau_{if}} = \frac{\Omega}{(2\pi)^3}\int d\mathbf{k}\frac{\pi}{\varepsilon\omega\Omega}[|\hat{e}_x\mathbf{p}_{if}|^2 + |\hat{e}_y\mathbf{p}_{if}|^2 + |\hat{e}_z\mathbf{p}_{if}|^2] \times \delta(E_i - E_f - \hbar\omega), \tag{A2}$$

where $\varepsilon=\varepsilon_0\varepsilon_r$; or, using Eq. (8) for the transition strength

$$\frac{1}{\tau_{if}} = \frac{\Omega}{(2\pi)^3}\int d\mathbf{k}\frac{\pi}{\varepsilon\omega\Omega} f_{if}(\hbar\omega). \tag{A3}$$

After integration ($d\mathbf{k} \rightarrow 4\pi k^2 dk$), using $\omega = ck/\bar{n}$ and $\bar{n}^2 = \varepsilon_r$ the final result reads

$$\frac{1}{\tau_{if}} = \frac{4}{3}\frac{\bar{n}(E_i - E_f)}{\pi\hbar^2 c^3 \varepsilon_0}[|\hat{e}_x \cdot \mathbf{p}_{if}|^2 + |\hat{e}_y \cdot \mathbf{p}_{if}|^2 + |\hat{e}_z \cdot \mathbf{p}_{if}|^2], \tag{A4}$$

where factor (4/3) comes from averaging over all possible light directions and spin degenerate transitions between i and f. In Figs. 11(a)–11(c) the momentum matrix elements, (d)–(f) the transition strength taking into account only the states at the $K_z=0$, and (g)–(i) the transition strength summed over all K_z states are given. The momentum matrix elements corresponding to CB→IB and IB→VB are $|\hat{e}_x\mathbf{p}_{e_1,e_0}|^2/P_0^2 = 0.044$ and $|\hat{e}_x\mathbf{p}_{e_0,h_0}|^2/P_0^2 = 0.223$ (in units of bulk interband momentum matrix element, equal to $P_0=9.37$ eV Å for InAs). Those intensities corresponds to transition energies: $E_{e_1} - E_{e_0} = 117.3$ meV and $E_{e_0} - E_{h_0} = 1.192$ eV, respectively. As can be seen from Figs. 11(a) and 11(b), for both transitions the $|\hat{e}_z\mathbf{p}_{if}|^2$ is negligible, and due to symmetry reasons $|\hat{e}_y\mathbf{p}_{if}|^2 = |\hat{e}_x\mathbf{p}_{if}|^2$. Next we express the radiative transition times in terms of the value of transition strength at energy that corresponds to the transition energy between states i and f, i.e., $\hbar\omega = E_i - E_f$. According Eq. (8), we can write: $\bar{f}_{if}(\hbar\omega = E_i - E_f) = \int |\hat{\mathbf{e}}\cdot\mathbf{p}_{if}|^2 \delta(E_i - E_f - \hbar\omega) d\hbar\omega = |\hat{\mathbf{e}}\cdot\mathbf{p}_{if}|^2 \cdot 1$. The ratio

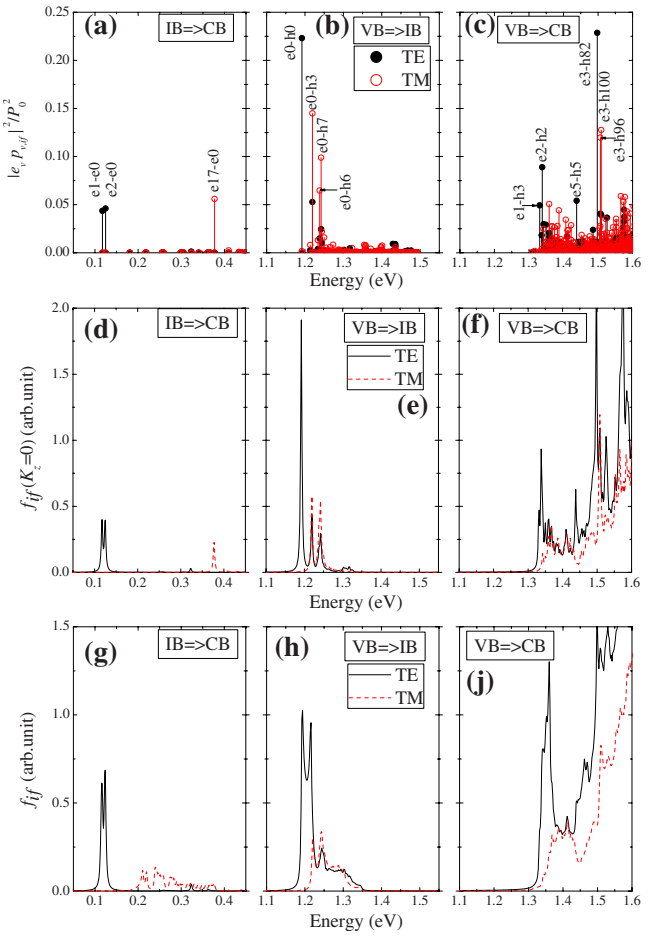

FIG. 11. (Color online) Momentum matrix elements of the QD array with vertical periodicity $d_z=5$ nm at $K_z=0$: (a) IB→CB transitions, (b) VB→IB transitions, (c) VB→CB transitions; the transition strength for the same array at the band edge $K_z=0$: (d) IB→CB transitions, (e) VB→IB transitions, (f) VB→CB transitions; and the transition strength for the same array summed over all K_z states: (g) IB→CB transitions, (h) VB→IB transitions, (j) VB→CB transitions. Both the TE (solid symbol or solid line) and TM (open symbol or dashed line) polarizations are shown.

between CB→IB and IB→VB radiative transition times, after noting from Figs. 11(a) and 11(b) that for these transitions $|\hat{e}_z\mathbf{p}_{if}|^2 \ll |\hat{e}_x\mathbf{p}_{if}|^2$ can be expressed in terms of the transition strength as

$$\frac{\tau_{e_1,e_0}}{\tau_{e_0,h_0}} = \frac{E_{e_0} - E_{h_0}}{E_{e_1} - E_{e_0}}\left(\frac{\bar{f}_{e_0,h_0}}{\bar{f}_{e_1,e_0}}\right) \approx \frac{E_{e_0} - E_{h_0}}{E_{e_1} - E_{e_0}}\left(\frac{|\hat{e}_x\mathbf{p}_{e_0,h_0}|^2}{|\hat{e}_x\mathbf{p}_{e_1,e_0}|^2}\right) \approx 52. \tag{A5}$$

In Figs. 11(a) and 11(d) the additional peak due to $|\hat{e}_z\mathbf{p}_{ij}|^2$ momentum matrix element (TM polarization) can be identified at the energy ~0.25 eV above the double peak that corresponds to $e_1 \rightarrow e_0$ and $e_2 \rightarrow e_0$ transitions. All these peaks in the intraband spectra have been previously observed in the single InAs/GaAs QD structures, both theoretically and experimentally.[91–93] The peak in the intraband spectra at ~0.37 eV also enables to identify the fist few, optically

strongest, minibands as depicted in Fig. 3. It is interesting to note that, after summation over K_z in the first Brillouin zone of the QD array, this peak disappears, Fig. 11(g). This suggests its very strong variation with K_z inside the miniband. The momentum matrix elements $|\hat{e}_x \mathbf{p}_{e_1,e_0}|^2$ and $|\hat{e}_x \mathbf{p}_{e_2,e_0}|^2$ are much less sensitive on K_z. Strong variation in the momentum matrix elements inside the QD array minibands has already been reported.[41,62] This indicates the importance of the integration over K_z in calculation of the absorption spectra of QD arrays.

The relation between the absorption coefficient, Eq. (7), and radiative transition time given by Eq. (A4) can be established via the transition strength as

$$\alpha(\hbar\omega_{if}) \propto \frac{1}{\omega_{if}} f_{if}(\hbar\omega_{if}) \propto \frac{1}{\omega_{if}\tau_{if}(E_i - E_f)}. \tag{A6}$$

Using values at the $K_z=0$ as $\omega^{\mathrm{VB}(h_0)\to\mathrm{IB}(e_0)} \approx 10 \times \omega^{\mathrm{IB}(e_0)\to\mathrm{CB}(e_1)}$, $|E_{\mathrm{VB}(h_0)} - E_{\mathrm{IB}(e_0)}| \approx 10 \times |E_{\mathrm{IB}(e_0)} - E_{\mathrm{CB}(e_1)}|$, and $\tau_{\mathrm{CB}(e_1),\mathrm{IB}(e_0)} \approx 50 \times \tau_{\mathrm{IB}(e_0),\mathrm{VB}(h_0)}$ it follows: $\alpha^{\mathrm{IB}(e_0)\to\mathrm{CB}(e_1)} \approx 2 \times \alpha^{\mathrm{VB}(h_0)\to\mathrm{IB}(e_0)}$. As can be seen comparing Figs. 11(d), 11(e), 11(g), and 11(h), the relative change in the ration between transition strengths, $f_{\mathrm{IB}(e_0),\mathrm{CB}(e_1)}/f_{\mathrm{VB}(h_0),\mathrm{IB}(e_0)}$, at the $K_z=0$ and after summation over all K_z values, another factor of ~ 2 can be extracted. Finally one gets $\alpha^{\mathrm{IB}(e_0)\to\mathrm{CB}(e_1)} \approx 4 \times \alpha^{\mathrm{VB}(h_0)\to\mathrm{IB}(e_0)}$, assuming integration over all K_z states which correspond to results shown in Fig. 6.

APPENDIX B: DERIVATION OF THE COULOMB INTEGRALS IN QD ARRAY

Detailed description of how the Coulomb integrals are evaluated in the system with periodic boundary conditions is given in Ref. 47. Here we present just the final results. By grouping the corresponding wave functions appearing in Eq. (11) as

$$B_{ij}(\mathbf{r}) = \psi_i^*(\mathbf{r})\psi_j(\mathbf{r}) \tag{B1}$$

and expressing the Coulomb potential as $V(u)=e^2/4\pi\epsilon u$, where u is the distance and ϵ is the static dielectric constant, the Coulomb integral Eq. (11), can be rewritten as

$$J(i,j;k,l) = \int d\mathbf{r}_1 \int d\mathbf{r}_2 B_{ik}(\mathbf{r}_1) V(|\mathbf{r}_1 - \mathbf{r}_2|) B_{jl}(\mathbf{r}_2). \tag{B2}$$

Introducing the plane-wave expansion of $B_{ij}(\mathbf{r})$ as

$$B_{ij}(\mathbf{r}) = \sum_{\mathbf{k}} B_{ij}(\mathbf{k}) e^{i\mathbf{k}\cdot\mathbf{r}} \tag{B3}$$

and after using the Fourier transform of the Coulomb potential $\mathcal{F}[V(u)]=e^2/\epsilon k^2$, the expression for the Coulomb integral in inverse space becomes

$$J(i,j;k,l) = \Omega\left(\frac{e^2}{\epsilon}\right) \sum_{\mathbf{k}} \frac{B_{ik}(\mathbf{k}) B_{jl}(-\mathbf{k})}{k^2}, \tag{B4}$$

where $B_{ij}(\mathbf{k})$ can be expressed in terms of the coefficients, $A_{i,\mathbf{k}}$, in the plane-wave expansion of the envelope functions (see Sec. II B) as

$$B_{ij}(\mathbf{k}) = \sum_{\mathbf{k}_1} A^*_{i,\mathbf{k}_1} A_{j,\mathbf{k}_1+\mathbf{k}}, \tag{B5}$$

and $\Omega = L_x \times L_y \times L_z$ is the volume of the supercell as defined in Sec. II B.

In order to understand the difference between two expressions, Eqs. (B2) and (B4), one can interpret the initial expression, Eq. (B2), if calculated in direct space, as energy of the electrostatic interaction between the complex charges $B_{ik}(\mathbf{r})$ and $B_{jl}(\mathbf{r})$, both being located in volume Ω. On the other hand, the expression Eq. (B4), is the energy of electrostatic interaction between $B_{ik}(\mathbf{r})$ located in volume Ω and $B_{jl}(\mathbf{r})$, located in the whole space with periodicity of the box Ω. Therefore, the Coulomb integrals $J(i,j;k,l)$ calculated according to Eq. (B4) represent the interactions between the charge $B_{ik}(\mathbf{r})$ of a single quantum dot and periodically replicated charges $B_{jl}(\mathbf{r})$ of neighboring periodically replicated dots in the array.

To avoid the undesired interaction of replicas in the nonperiodic (x and y) directions,[94] we performed the Coulomb integral calculations on the box size with those two dimensions extended as explained in Ref. 47.

*stanko.tomic@stfc.ac.uk

[1] W. Shockley and H. J. Queisser, J. Appl. Phys. **32**, 510 (1961).
[2] M. Green, Prog. Photovoltaics **9**, 123 (2001).
[3] A. Nozik, Physica E **14**, 115 (2002).
[4] R. R. King, Nat. Photonics **2**, 284 (2008).
[5] A. Luque and A. Martí, Phys. Rev. Lett. **78**, 5014 (1997).
[6] A. Luque, A. Marti, and A. J. Nozik, MRS Bull. **32**, 236 (2007).
[7] A. Luque and A. Marti, Adv. Mater. **22**, 160 (2010).
[8] A. Martí, E. Antolín, C. R. Stanley, C. D. Farmer, N. López, P. Díaz, E. Cánovas, P. G. Linares, and A. Luque, Phys. Rev. Lett. **97**, 247701 (2006).
[9] A. Luque and A. Marti, Prog. Photovoltaics **9**, 73 (2001).
[10] L. Cuadra, A. Marti, and A. Luque, IEEE Trans. Electron Devices **51**, 1002 (2004).
[11] A. Luque, A. Marti, N. Lopez, E. Antolin, E. Canovas, C. Stanley, C. Farmer, L. Caballero, L. Cuadra, and J. Balenzategui, Appl. Phys. Lett. **87**, 083505 (2005).
[12] A. Luque, A. Marti, E. Antolin, and C. Tablero, Physica B **382**, 320 (2006).
[13] S. P. Bremner, M. Y. Levy, and C. B. Honsberg, Appl. Phys. Lett. **92**, 171110 (2008).
[14] S. A. Blokhin, A. V. Sakharov, A. M. Nadtochy, A. S. Pauysov, M. V. Maximov, N. N. Ledentsov, A. R. Kovsh, S. S. Mikhrin, V. M. Lantratov, S. A. Mintairov, N. A. Kaluzhniy, and M. Z. Shvarts, Semiconductors **43**, 514 (2009).
[15] Q. Xie, A. Madhukar, P. Chen, and N. P. Kobayashi, Phys. Rev. Lett. **75**, 2542 (1995).
[16] D. M. Bruls, P. M. Koenraad, H. W. M. Salemink, J. H. Wolter, M. Hopkinson, and M. S. Skolnick, Appl. Phys. Lett. **82**, 3758 (2003).

[17] A. Martí, N. López, E. Antolín, E. Cánovas, A. Luque, C. R. Stanley, C. D. Farmer, and P. Díaz, Appl. Phys. Lett. **90**, 233510 (2007).
[18] S. M. Hubbard, C. D. Cress, C. G. Bailey, R. P. Raffaelle, S. G. Bailey, and D. M. Wilt, Appl. Phys. Lett. **92**, 123512 (2008).
[19] D. Alonso-Álvarez, A. G. Taboada, J. M. Ripalda, B. Alén, Y. González, L. González, J. M. García, F. Briones, A. Martí, A. Luque, A. M. Sánchez, and S. I. Molina, Appl. Phys. Lett. **93**, 123114 (2008).
[20] R. Oshima, A. Takata, and Y. Okada, Appl. Phys. Lett. **93**, 083111 (2008).
[21] K. Akahane, N. Yamamoto, and T. Kawanishi, International Conference on Indium Phosphide and Related Materials, Newport Beach, CA, May 10-14, 2009 (unpublished), p. 73.
[22] K. Akahane, N. Yamamoto, and T. Kawanishi, IEEE Photon. Technol. Lett. **22**, 103 (2010).
[23] Z. Fan, H. Razavi, J.-w. Do, A. Moriwaki, O. Ergen, Y.-L. Chueh, P. W. Leu, J. C. Ho, T. Takahashi, L. A. Reichertz, S. Neale, K. Yu, M. Wu, J. W. Ager, and A. Javey, Nature Mater. **8**, 648 (2009).
[24] D. Guimard, R. Morihara, D. Bordel, K. Tanabe, Y. Wakayama, M. Nishioka, and Y. Arakawa, Appl. Phys. Lett. **96**, 203507 (2010).
[25] R. Strandberg and T. W. Reenaas, J. Appl. Phys. **105**, 124512 (2009).
[26] A. Marti, L. Cuadra, and A. Luque, IEEE Trans. Electron Devices **49**, 1632 (2002).
[27] J. M. Luttinger and W. Kohn, Phys. Rev. **97**, 869 (1955).
[28] E. O. Kane, J. Phys. Chem. Solids **1**, 249 (1957).
[29] E. O. Kane, Semicond. Semimetals **1**, 75 (1966).
[30] M. Cardona and F. H. Pollak, Phys. Rev. **142**, 530 (1966).
[31] S. Richard, F. Aniel, and G. Fishman, Phys. Rev. B **70**, 235204 (2004).
[32] D. Rideau, M. Feraille, L. Ciampolini, M. Minondo, C. Tavernier, H. Jaouen, and A. Ghetti, Phys. Rev. B **74**, 195208 (2006).
[33] B. A. Foreman, Phys. Rev. B **76**, 045327 (2007).
[34] I. Saïdi, S. B. Radhia, and K. Boujdaria, J. Appl. Phys. **107**, 043701 (2010).
[35] I. Vurgaftman, J. R. Meyer, and L. R. Ram-Mohan, J. Appl. Phys. **89**, 5815 (2001).
[36] G. L. Bir and G. E. Pikus, *Symmetry and Strain-Induced Effects in Semiconductors* (Wiley, New York, 1974).
[37] J. P. Loehr, *Physics of Strained Quantum Well Lasers* (Kluwer Academic, Dortrecht, 1998).
[38] C. R. Pidgeon and R. N. Brown, Phys. Rev. **146**, 575 (1966).
[39] C. Pryor, Phys. Rev. B **57**, 7190 (1998).
[40] O. Stier, M. Grundmann, and D. Bimberg, Phys. Rev. B **59**, 5688 (1999).
[41] S. Tomić, T. S. Jones, and N. M. Harrison, Appl. Phys. Lett. **93**, 263105 (2008).
[42] E. Canovas, A. Marti, N. Lopez, E. Antolin, P. Linares, C. Farmer, C. Stanley, and A. Luque, Thin Solid Films **516**, 6943 (2008).
[43] E. Canovas, A. Marti, D. Fuertes-Marron, E. Antolin, and A. Luque, Proceedings of the 23rd European Photovoltaic Conference, Valencia, September, 2008 (unpublished), p. 298.
[44] M. A. Cusack, P. R. Briddon, and M. Jaros, Phys. Rev. B **54**, R2300 (1996).
[45] N. Vukmirović, D. Indjin, V. D. Jovanović, Z. Ikonić, and P. Harrison, Phys. Rev. B **72**, 075356 (2005).
[46] S. Tomić, A. G. Sunderland, and I. J. Bush, J. Mater. Chem. **16**, 1963 (2006).
[47] N. Vukmirović and S. Tomić, J. Appl. Phys. **103**, 103718 (2008).
[48] A. D. Andreev, J. R. Downes, D. A. Faux, and E. P. O'Reilly, J. Appl. Phys. **86**, 297 (1999).
[49] S.-S. Li, J.-B. Xia, Z. L. Yuan, Z. Y. Xu, W. Ge, X. R. Wang, Y. Wang, J. Wang, and L. L. Chang, Phys. Rev. B **54**, 11575 (1996).
[50] A. D. Andreev, Proc. SPIE **3284**, 151 (1998).
[51] O. L. Lazarenkova and A. A. Balandin, J. Appl. Phys. **89**, 5509 (2001).
[52] J. W. Kłos and M. Krawczyk, J. Appl. Phys. **106**, 093703 (2009).
[53] R. L. Kronig and W. G. Penney, Proc. R. Soc. London, Ser. A **130**, 499 (1931).
[54] M. Grundmann, J. Christen, N. N. Ledentsov, J. Böhrer, D. Bimberg, S. S. Ruvimov, P. Werner, U. Richter, U. Gösele, J. Heydenreich, V. M. Ustinov, A. Y. Egorov, A. E. Zhukov, P. S. Kopev, and Z. I. Alferov, Phys. Rev. Lett. **74**, 4043 (1995).
[55] V. Popescu, G. Bester, M. C. Hanna, A. G. Norman, and A. Zunger, Phys. Rev. B **78**, 205321 (2008).
[56] The TE means that the optical field is polarized along any of, $\hat{e}_x+\hat{e}_y$, directions that are "in plane" of the structure and is perpendicular to the QD array growth axis; TM means that the optical field is polarized along, $\hat{e}_z$, direction parallel to the QD array growth axes.
[57] R. J. Elliott, Phys. Rev. **108**, 1384 (1957).
[58] T. Takagahara, Phys. Rev. B **47**, 4569 (1993).
[59] P. Y. Yu and M. Cardona, *Fundamentals of Semiconductors* (Springer, New York, 2001).
[60] F. Capasso, C. Sirtori, J. Faist, D. Sivco, S. Chu, and A. Cho, Nature (London) **358**, 565 (1992).
[61] D. Gershoni, J. Oiknine-Schlesinger, E. Ehrenfreund, D. Ritter, R. A. Hamm, and M. B. Panish, Phys. Rev. Lett. **71**, 2975 (1993).
[62] S. Tomić, N. Harrison, and T. Jones, Proceedings of the 23rd European Photovoltaic Conference, Valencia, September, 2008, p. 522.
[63] N. Vukmirović, Z. Ikonić, I. Savić, D. Indjin, and P. Harrison, J. Appl. Phys. **100**, 074502 (2006).
[64] L. Asryan and R. Suris, Semicond. Sci. Technol. **11**, 554 (1996).
[65] L. Asryan, M. Grundmann, N. Ledentsov, O. Stier, R. Suris, and D. Bimberg, J. Appl. Phys. **90**, 1666 (2001).
[66] V. Popescu, G. Bester, and A. Zunger, Appl. Phys. Lett. **95**, 023108 (2009).
[67] W. van Roosbroeck and W. Shockley, Phys. Rev. **94**, 1558 (1954).
[68] L.-W. Wang, Energy Environ. Sci. **2**, 944 (2009).
[69] L.-W. Wang, M. Califano, A. Zunger, and A. Franceschetti, Phys. Rev. Lett. **91**, 056404 (2003).
[70] G. A. Narvaez, G. Bester, and A. Zunger, Phys. Rev. B **74**, 075403 (2006).
[71] T. Müller, F. F. Schrey, G. Strasser, and K. Unterrainer, Appl. Phys. Lett. **83**, 3572 (2003).
[72] T. B. Norris, K. Kim, J. Urayama, Z. K. Wu, J. Singh, and P. K. Bhattacharya, J. Phys. D **38**, 2077 (2005).
[73] G. Makov and M. C. Payne, Phys. Rev. B **51**, 4014 (1995).
[74] J. Even, L. Pedesseau, F. Dore, and S. Boyer-Richard, Opt. Quantum Electron. **40**, 1233 (2008).

[75] M. T. Crowley, I. P. Marko, N. F. Masse, A. D. Andreev, S. Tomic, S. J. Sweeney, E. P. O'Reilly, and A. R. Adams, IEEE J. Sel. Top. Quantum Electron. **15**, 799 (2009).
[76] S. J. Sweeney, T. Higashi, A. Andreev, A. R. Adams, T. Uchida, and T. Fujii, Phys. Status Solidi B **223**, 573 (2001).
[77] S. J. Sweeney, A. R. Adams, M. Silver, E. P. O'Reilly, J. R. Watling, A. B. Walker, and P. J. A. Thijs, Phys. Status Solidi B **211**, 525 (1999).
[78] A. D. Andreev and E. P. O'Reilly, Appl. Phys. Lett. **84**, 1826 (2004).
[79] M. Califano (private communication).
[80] D. Harrison, R. Abram, and S. Brand, J. Appl. Phys. **85**, 8178 (1999).
[81] M. Wimmer, S. V. Nair, and J. Shumway, Phys. Rev. B **73**, 165305 (2006).
[82] G. Mahan, *Many-Particle Physics* (Kluwer Academic, New York, 2000).
[83] M. A. Stroscio and M. Dutta, *Phonons in Nanostructures* (Cambridge University Press, Cambridge, 2001).
[84] S. Hameau, Y. Guldner, O. Verzelen, R. Ferreira, G. Bastard, J. Zeman, A. Lemaître, and J. M. Gérard, Phys. Rev. Lett. **83**, 4152 (1999).
[85] X.-Q. Li, H. Nakayama, and Y. Arakawa, Phys. Rev. B **59**, 5069 (1999).
[86] O. Verzelen, R. Ferreira, and G. Bastard, Phys. Rev. B **62**, R4809 (2000).
[87] S. Sauvage, P. Boucaud, R. P. S. M. Lobo, F. Bras, G. Fishman, R. Prazeres, F. Glotin, J. M. Ortega, and J.-M. Gérard, Phys. Rev. Lett. **88**, 177402 (2002).
[88] X. Q. Li and Y. Arakawa, Phys. Rev. B **57**, 12285 (1998).
[89] E. A. Zibik, L. R. Wilson, R. P. Green, G. Bastard, R. Ferreira, P. J. Phillips, D. A. Carder, J.-P. R. Wells, J. W. Cockburn, M. S. Skolnick, M. J. Steer, and M. Hopkinson, Phys. Rev. B **70**, 161305(R) (2004).
[90] V. Aroutiounian, S. Petrosyan, A. Khachatryan, and K. Touryan, J. Appl. Phys. **89**, 2268 (2001).
[91] S. Sauvage, P. Boucaud, F. Julien, J. Gerard, and V. ThierryMieg, Appl. Phys. Lett. **71**, 2785 (1997).
[92] V. Aleshkin *et al.*, Proc. SPIE **5023**, 209 (2002).
[93] L. E. Vorobjev, D. A. Firsov, V. A. Shalygin, N. K. Fedosov, V. Y. Panevin, A. Andreev, V. M. Ustinov, G. E. Cirlin, V. A. Egorov, A. A. Tonkikh, F. Fossard, M. Tchernycheva, K. Moumanis, F. H. Julien, S. Hanna, A. Seilmeier, and H. Sigg, Semicond. Sci. Technol. **21**, 1341 (2006).
[94] C. A. Rozzi, D. Varsano, A. Marini, E. K. U. Gross, and A. Rubio, Phys. Rev. B **73**, 205119 (2006).